PAPER

Check for updates

Synthesis and luminescence properties of Eu^{3+}-activated BiF$_3$ nanoparticles for optical thermometry and fluorescence imaging in rice root

Peng Du, †[a] Yunfei Wu†*[b] and Jae Su Yu *[a]

The luminescence, optical thermometric properties, phytotoxicity, and fluorescence imaging in plant cells of Eu^{3+}-activated BiF$_3$ nanoparticles were systematically studied. Under the excitation of near-ultraviolet light, the prepared compounds emitted visible red light arising from the intra-4f transitions of Eu^{3+} ions. By employing the fluorescence intensity ratio technique, the temperature sensing performance of the synthesized nanoparticles was investigated and the maximum sensitivity was demonstrated to be 3.4 × 10^{-5} K^{-1} at 443 K. Furthermore, the rice root, which was treated with Eu^{3+}-activated BiF$_3$ nanoparticles, showed similar primary root elongation and crown root number to the seedlings cultivated in the MS0 medium without nanoparticles, indicating the relatively low phytotoxicity of the resultant samples to the rice root. Additionally, the results of the toxicity-related gene levels and phenotypes also demonstrated the low phytotoxicity of the as-prepared nanoparticles to the plant cells. Ultimately, with the help of the red emission of Eu^{3+} ions, the studied compounds were found to be accumulated in the division and differentiation regions of the rice root rather than transferred to the above-ground tissues. These results suggest that the Eu^{3+}-activated BiF$_3$ nanoparticles may have potential applications in non-invasive optical temperature sensors and fluorescence probes in plant cells.

1. Introduction

Recently, luminescent nanoparticles in which trivalent rare-earth ions act as activators have attracted great attention because of their practical applications in various fields, such as indoor illumination, in nano-thermometers, drug delivery, fluorescence imaging in plant cells, photovoltaic generation, and field emission displays.[1–10] Among these trivalent rare-earth ions, the Eu^{3+} ion, which is regarded as a promising red-emitting activator owing to its featured emission originating from the intra-4f transition, has been extensively studied.[11–13] It was reported that NaEuF$_4$ nanoparticles, which emit dazzling red emission, are suitable for optical thermometry using a fluorescence intensity ratio (FIR) technique.[14] Shi *et al.* revealed that Eu^{3+}-activated β-NaGdF$_4$ nanoparticles with impressive luminescence properties have potential applications in *in vivo* bioimaging.[15] Furthermore, in our previous work, we also found that NaBiF$_4$:Eu^{3+} nanoparticles are promising candidates for simultaneous white light-emitting diodes and field emission displays.[16] Despite these achievements, more efforts are still required to further investigate the luminescence

performance of Eu^{3+} ions and their applications. In addition, it is widely accepted that the luminescence properties of rare-earth ion-activated materials are strongly dependent on the host matrix. In general, a lower phonon energy results in a higher radiative transition probability and a higher luminescence efficiency.[17,18] To date, the fluorides, such as NaYF$_4$, NaLaF$_4$, BiF$_3$, and LaF$_3$, have been widely investigated as luminescent host materials and some admirable results have been obtained.[19–22] Nevertheless, the exploration of the luminescence properties and potential applications of BiF$_3$ is still insufficient. For the sake of filling this gap, BiF$_3$ was selected as the luminescent host material.

Bioimaging is a vital diagnostic method to realize the investigation and visualization of biological interaction among living cells. In particular, interest in fluorescence imaging in plant cells is increasing since it can help us to comprehend the growth of plants. Unfortunately, the conventional biological probe, for example, one using a fluorescent dye, suffers from inhibited luminescence emission intensity in the plant cells due to the aggregation-induced quenching effect which limits its applications.[23,24] In comparison, inorganic luminescent nanoparticles exhibit high photochemical stability and visible emission, and they can be directly excited by a commercial light-emitting diode chip. Furthermore, the nanoparticles show stable luminescence even in some harsh environments, for example, in an aqueous environment, which makes the nanoparticles suitable for fluorescence imaging in plant cells.[25,26] In

[a]*Department of Electronic Engineering, Kyung Hee University, Yongin-si 17104, Republic of Korea. E-mail: jsyu@khu.ac.kr*

[b]*Crop Biotech Institute, Graduate School of Biotechnology, Kyung Hee University, Yongin 17104, Republic of Korea. E-mail: yunfeisky85@gmail.com*

† P. Du and Y. Wu contributed equally to this work.

this work, Eu^{3+}-activated BiF_3 nanoparticles were synthesized *via* a simple chemical precipitation method. The phase composition, morphology, and luminescence of the resultant nanoparticles were characterized. Using the FIR technique, the optical thermometric properties of the prepared samples were studied. Moreover, the effect of the Eu^{3+}-activated BiF_3 nanoparticles on the phytotoxicity and the development of rice root at the young seedling stage was systematically discussed. Ultimately, the transcript levels of toxicity-related genes and fluorescence imaging in the rice root cells were investigated in detail.

2. Experimental section

2.1 Synthesis of Eu^{3+}-activated BiF_3 nanoparticles

$Bi(NO_3)_3 \cdot 5H_2O$ (98%), NH_4F (99.99%), and $Eu(NO_3)_3 \cdot 5H_2O$ (99.9%) were employed as the starting materials to prepare the Eu^{3+}-activated BiF_3 (BiF_3:Eu^{3+}) nanoparticles. To synthesize the BiF_3:Eu^{3+} nanoparticles, a facile chemical precipitation method was applied. In brief, 0.95 mmol $Bi(NO_3)_3 \cdot 5H_2O$ and 0.05 mmol $Eu(NO_3)_3 \cdot 5H_2O$ were dissolved in 10 ml of ethylene glycol to form solution I. Meanwhile, 3 mmol of NH_4F was dissolved into 20 ml of ethylene glycol to generate solution II. Subsequently, solution I was slowly dropped into solution II and stirred for 1 min at room temperature. Ultimately, the final compounds were obtained by means of centrifugation, washing with ethanol and deionized water three times to remove remaining reagent, and then drying at 80 °C for 6 h in air.

2.2 Characterization of the resultant nanoparticles

An X-ray diffractometer (Bruker D8) with Cu Kα radiation ($\lambda = 1.5406$ Å) at a current of 40 mA and a voltage of 40 kV was used to examine the phase composition of the final products. The morphology of the resultant samples was characterized by using a high-resolution field-emission scanning electron microscope (HR-FE-SEM; LEO SUPRA 5) with an accelerating voltage of 10 kV and a resolution of 3.0 nm. The luminescence properties of the studied nanoparticles were investigated by using a fluorescence spectrometer (Scinco FluroMate FS5). A thermocouple (NOVA ST540) was employed to adjust the temperature around the nanoparticles.

2.3 Plant materials and growth conditions

Japonica rice (*Oryza sativa* 'Dongjin') plants were grown in a controlled environment room. On the basis of previous literature, seeds were germinated on a Murashige and Skoog (MS) medium without or with different amounts of BiF_3:Eu^{3+} nanoparticles at a temperature of 28 °C under continuous light exposure.[27]

2.4 Localization of RFP

After treatment with the BiF_3:Eu^{3+} nanoparticles, rice root samples at 4 days after germination (DAG) were cleared following the method of Sabatini *et al.* and analyzed by using a microscope (OLYMPUS BX61; Olympus, Tokyo, Japan) under bright DIC-field and RFP-field illumination.[28] Root tips at the

same stage were fixed in 3% (w/v) paraformaldehyde, 5% (v/v) acetic acid, and 63% (v/v) ethanol. Following ethanol dehydration, the samples were embedded in Technovit Embedding Kits 7100 (Germany) and cut into 5 μm sections by using a microtome (Leica RM2265).[29] The sections were imaged both in bright DIC-field and RFP-field channels.

2.5 RT-PCR analyses

The total RNA was isolated from the total root of the plants at 4 DAG.[29] According to a previous description, the cDNAs were prepared and quantitative RT-PCR was carried out.[29,30] The internal control was rice *UBQ5* (*LOC_Os01g22490*). All experiments were conducted at least three times, with six samples taken at each point. To ensure primer specificity, we performed the experiments when the melting curve showed a single sharp peak. The PCR products were sequenced to verify the specificity of the reaction.[29,30]

2.6 Statistical analysis

Students' *t*-tests were applied to demonstrate any statistically significant differences between the values achieved from the control and treatment experiments.

3. Results and discussion

3.1 Phase structure, morphology, and luminescence properties of the BiF_3:Eu^{3+} nanoparticles

The phase composition and crystal structure of the resultant nanoparticles were characterized by X-ray diffraction (XRD). The XRD pattern presented in Fig. 1(a) reveals that all the detected diffraction peaks are in good agreement with the peaks for cubic BiF_3 (JCPDS#39-0345), implying that the Eu^{3+}-activated BiF_3 nanoparticles possessed a pure cubic phase and the Eu^{3+} ions were successfully incorporated into the BiF_3 host lattice. The FE-
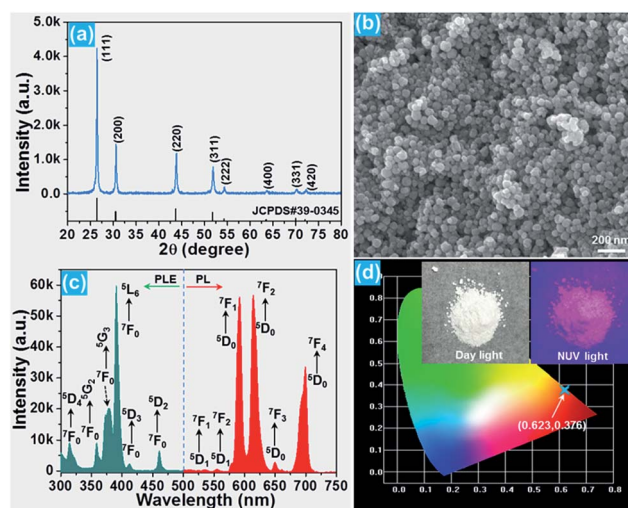

Fig. 1 (a) XRD pattern, (b) FE-SEM image, (c) PL excitation ($\lambda_{em} = 615$ nm) and emission ($\lambda_{ex} = 391$ nm) spectra, and (d) CIE diagram of the BiF_3:Eu^{3+} nanoparticles. The inset shows the images of the resultant nanoparticles under day light and NUV light.

SEM image confirmed that the synthesized samples were composed of homogeneously spherical nanoparticles with an average size of ~50 nm (Fig. 1(b)). Furthermore, the photoluminescence (PL) excitation and emission spectra were recorded to analyze the room-temperature luminescence properties of the prepared nanoparticles. As presented, the excitation spectrum monitored at 615 nm consisted of several narrow peaks located at around 314, 358, 379, 391, 413, and 461 nm corresponding to the $^7F_0 \rightarrow {}^5D_4$, $^7F_0 \rightarrow {}^5G_2$, $^7F_0 \rightarrow {}^5G_3$, $^7F_0 \rightarrow {}^5L_6$, $^7F_0 \rightarrow {}^5D_3$, and $^7F_0 \rightarrow {}^5D_2$ transitions, respectively (Fig. 1(c)).[16,31] In comparison, the excitation band at 391 nm exhibited the strongest intensity, suggesting that the prepared samples can be excited by near-ultraviolet (NUV) light. Under excitation at 391 nm, the BiF_3:Eu^{3+} nanoparticles emitted the featured emissions of Eu^{3+} ions and the emissions centered at 591 nm ($^5D_0 \rightarrow {}^7F_1$), 615 nm ($^5D_0 \rightarrow {}^7F_2$), and 699 nm ($^5D_0 \rightarrow {}^7F_4$) were dominant in the emission spectrum. Apart from these dominant peaks, several weak emissions at around 535, 555, and 650 nm corresponding to the $^5D_1 \rightarrow {}^7F_1$, $^5D_1 \rightarrow {}^7F_2$, and $^5D_0 \rightarrow {}^7F_3$ transitions of Eu^{3+} ions were also detected, as presented in Fig. 1(c).[32,33] As shown in Fig. 1(d), the resultant nanoparticles can emit bright visible red emission and the corresponding Commission Internationale de l'Eclairage (CIE) coordinate was determined to be (0.623, 0.376) which was located in the red region.

3.2 Optical thermometric properties of the BiF_3:Eu^{3+} nanoparticles

On the basis of previous literature,[14,34] it is known that Eu^{3+} ions have a pair of thermally coupled levels of $^5D_0$ and $^5D_1$. As a consequence, electrons can be excited to the $^5D_1$ level from the $^5D_0$ level on increasing the temperature, leading to the variation in the emission intensities originating from the $^5D_1$ and $^5D_0$ levels at elevated temperature, which makes the Eu^{3+} ion-doped materials promising candidates for optical thermometry using the FIR technique. To explore the potential application of the studied samples, the temperature-dependent PL emission spectra of the Eu^{3+}-activated BiF_3 nanoparticles were measured. As shown, the emission bands scarcely changed with increasing the temperature, while the emission intensity showed a downward tendency when the temperature was increased from 303 to 443 K (Fig. 2(a)). From the recorded temperature-dependent PL emission spectra, the FIR values of the emissions arising from the thermally coupled levels of $^5D_1$ and $^5D_0$ were estimated and the corresponding results are shown in Fig. 2(b). It can be seen that the FIR value increased gradually with the increment of temperature and reached a maximum value of around 0.019 at 443 K. According to the theory proposed by Wade et al., the FIR values of the emissions originating from two thermally coupled levels can be expressed as:[35,36]

$$\mathrm{FIR} = \frac{I_U}{I_L} = A \exp\left(-\frac{\Delta E}{kT}\right) + B, \quad (1)$$

where I_U and I_L are the integrated emission intensities from the upper and lower excited levels, respectively, A and B are constants, ΔE refers to the energy gap, k is the Boltzmann
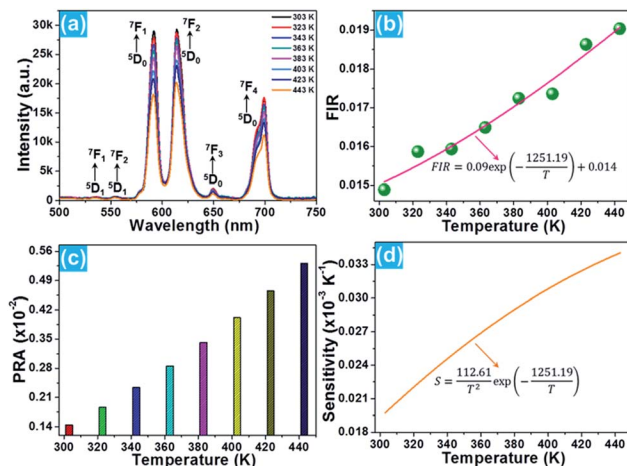

Fig. 2 (a) Temperature-dependent PL emission spectra of the BiF_3:Eu^{3+} nanoparticles. (b) FIR and (c) PRA values at different temperatures. (d) Sensor sensitivity as a function of temperature.

constant, and T is the temperature. As presented in Fig. 2(b), with the help of eqn (1), the calculated FIR value can be well fitted and the A, $\Delta E/k$, and B values were determined to be 0.09, 1251.19, and 0.014, respectively. As demonstrated above, the $^5D_1$ level can be populated from the $^5D_0$ level by means of thermal excitation, leading to the population redistribution between the $^5D_1$ and $^5D_0$ levels at high temperature. To further comprehend the temperature-induced population redistribution phenomenon, the temperature-induced population redistribution ability (PRA) was evaluated utilizing the following expression:[37,38]

$$\mathrm{PRA} = \frac{I_U}{I_U + I_L} = \frac{A}{A + \exp(\Delta E/kT)} \quad (2)$$

In this formula, I_U, I_L, A, ΔE, k, and T have the same meaning as described in eqn (1). Based on the fitting results, the PRA value was calculated, as depicted in Fig. 2(c). Clearly, the PRA value was as low as 0.0014 when the temperature was 303 K. However, on elevating the temperature, the PRA value increased sharply, reaching a maximum of 0.0053 at 443 K. This result further implies that the population between the $^5D_1$ and $^5D_0$ levels can be redistributed and the studied samples may have potential applications in optical thermometry by the FIR route.

For optical thermometry applications, the sensor sensitivity of the resultant samples should be investigated and it can be evaluated using the following formula:[39,40]

$$S = \frac{d(\mathrm{FIR})}{dT} = \frac{\Delta E}{kT^2}(\mathrm{FIR} - B) \quad (3)$$

With the help of eqn (3), the temperature-dependent sensor sensitivity was estimated, as shown in Fig. 2(d). As demonstrated, the sensor sensitivity exhibited an upward tendency with temperature, reaching a maximum of about 3.4×10^{-5} K^{-1} at 443 K. Clearly, the calculated sensor sensitivity was comparable to that of other optical sensing materials, such as

NaYbF$_4$:Tm^{3+}, KLuF$_4$:Tm^{3+}, and PbF$_2$:Tm^{3+}/Yb^{3+},[41–43] which further confirms that the Eu^{3+}-activated BiF$_3$ nanoparticles are suitable for optical thermometry using the FIR technique.

3.3 Phytotoxicity of the BiF$_3$:Eu^{3+} nanoparticles

For the purpose of studying the effect of the BiF$_3$:Eu^{3+} nanoparticles on the growth of rice root as well as their phytotoxicity to rice root, a series of wide type (WT) rice roots were cultivated in MS media without sucrose (MS0) containing various concentrations of BiF$_3$:Eu^{3+} nanoparticles. From the images of the cultivated rice roots (Fig. 3(a and b)), it is evident that the development of rice root was scarcely affected by the addition of the BiF$_3$:Eu^{3+} nanoparticles. Furthermore, the elongation speed of the primary root of the seedlings treated with BiF$_3$:Eu^{3+} nanoparticles was almost the same as that of the rice roots grown in the MS0 medium without nanoparticles, as depicted in Fig. 3(c). In addition, the number of crown roots was also hardly influenced by the introduction of the BiF$_3$:Eu^{3+} nanoparticles (Fig. 3(d)). These results revealed that the Eu^{3+}-activated BiF$_3$ nanoparticles possessed relatively low phytotoxicity to the rice root.

To investigate the phenotype of the rice root, the root tips, which were cultivated with different concentrations of BiF$_3$:Eu^{3+} nanoparticles, were stained using iodine–potassium (KI–I$_2$) and the corresponding results are presented in Fig. 4(a–e). The rice tip obtained in the MS0 medium without nanoparticles had a clear area surrounding the Quiescent Center (QC) cells, as shown in Fig. 4(a). Note that on increasing the content of the BiF$_3$:Eu^{3+} nanoparticles from 10 to 200 μM, little change occurred around the QC cells (Fig. 4(b–e)), further implying that the BiF$_3$:Eu^{3+} nanoparticles did little damage and had low

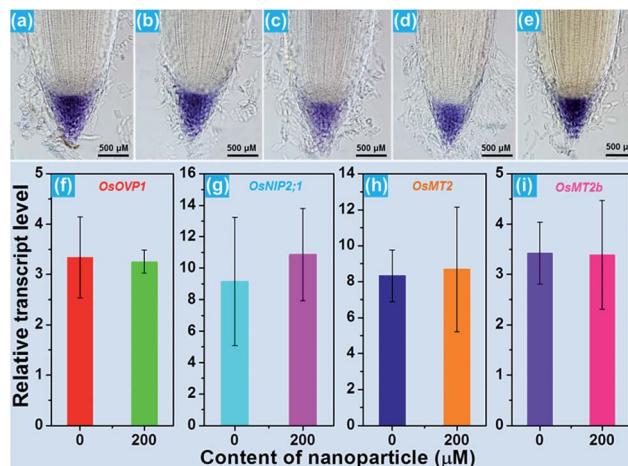Fig. 4   (a) Phenotypes of root tips stained by KI–I$_2$: (a) WT control, (b) WT treated with 10 μM nanoparticles, (c) WT treated with 50 μM nanoparticles, (d) WT treated with 100 μM nanoparticles, and (e) WT treated with 200 μM nanoparticles. Expression levels of phytotoxic genes relative to OsUBQ5: (f) *OsOVP1*, (g) *OsNIP2;1*, (h) *OsMT2*, and (i) *OsMT2b*.

phytotoxicity to the rice root. For the sake of verifying the low toxicity of the resultant nanoparticles to the rice root, the transcript levels of several toxicity-related genes were examined. As is known, some genes including *OsOVP1* (a vacuolar H$^+$-translocating inorganic pyrophosphatase), nodulin 26-like intrinsic protein (*OsNIP2;1*), metallothionein (*OsMT2*), and metallothionein 2b (*OsMT2b*) are phytotoxic to rice.[44–47] The transcript levels of the *OsOVP1*, *OsNIP2;1*, *OsMT2*, and *OsMT2b* genes are illustrated in Fig. 4(f–i). Compared with those of the seedlings grown in MS0 media, it is evident that the entire transcript levels of the recorded genes of the rice root treated with 200 μM nanoparticles barely changed. In particular, the transcript level of the *OsMT2b* gene of the rice root was nearly the same as that of the WT controlled sample (Fig. 4(i)). Generally, plants with a high transcript level of the *OsMT2b* gene exhibit a low level of hydrogen peroxide, low elongation of the primary root, and a large number of crown roots by cytokinin signaling.[46] Since the BiF$_3$:Eu^{3+} nanoparticle-treated rice root possessed the same transcript level of the *OsMT2b* gene as that of the seedlings grown in MS0 media without adding the synthesized nanoparticles, it is reasonable to consider that the resultant nanoparticles exhibited relatively low phytotoxicity to the rice root and had little influence on the growth of the rice root, which coincided well with the aforementioned results. These results suggested that the Eu^{3+}-activated BiF$_3$ nanoparticles with low toxicity may be employed as a fluorescence probe in plant cells.

3.4 Fluorescence imaging in rice root cells

As demonstrated above, the Eu^{3+}-activated BiF$_3$ nanoparticles can emit strong visible red emission under NUV light excitation and the red light can easily penetrate the plant tissues which makes them suitable for real-time detection of the location of the nanoparticles in the plant cells. To explore the
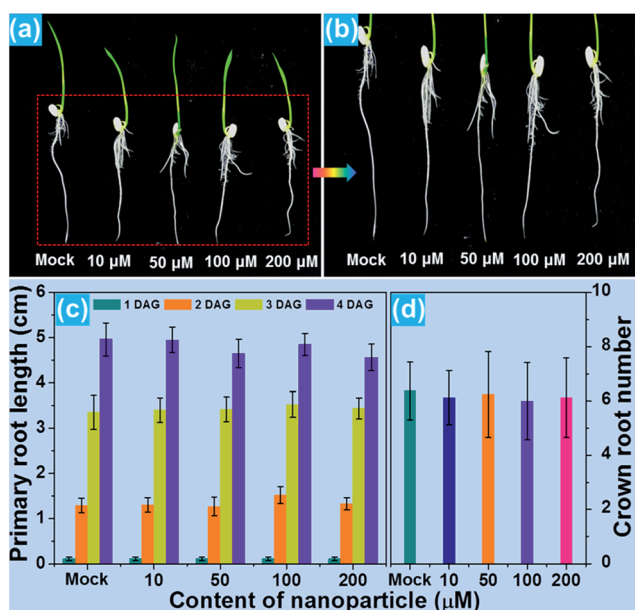

Fig. 3   (a and b) Images of plants grown in MS0 media containing different amounts of BiF$_3$:Eu^{3+} nanoparticles. (c) Primary root length and (d) crown root number as a function of concentration of BiF$_3$:Eu^{3+} nanoparticles.

transportation process of the resultant compounds as well as their location in the rice roots, *in vitro* fluorescence imaging was carried out. It can be seen that the rice tip cut from the rice root, which was cultivated in the MS0 medium without $BiF_3:Eu^{3+}$ nanoparticles, exhibited very weak RFP signals which were hardly observed by the naked eye when excited by 396 nm light, as presented in Fig. 5(a–c). In comparison, the rice tip treated with 200 μM $BiF_3:Eu^{3+}$ nanoparticles emitted a bright RFP signal in the red region under excitation at 396 nm (Fig. 5(d–f)). Note that the RFP signal is only present in the division and differentiation regions, while the root cap and mature region did not emit any RFP signals, as shown in Fig. 5(e and f), revealing that the $BiF_3:Eu^{3+}$ nanoparticles were only distributed in the division and differentiation regions rather than in the root cap and mature regions. To gain deeper insight into the distribution of the studied nanoparticles, the *in vitro* cross-sectional images of the root tips in the division and differentiation regions were detected and are depicted in Fig. 6. As shown in Fig. 6(a–c), the rice root grown in the MS0 medium without $BiF_3:Eu^{3+}$ nanoparticles did not show any clear RFP signals. However, after treatment with 200 μM $BiF_3:Eu^{3+}$ nanoparticles, the rice root tip emitted significant RFP signals, further confirming that the nanoparticles were located in the division and differentiation regions (Fig. 6(d–f)). As is known, small sized nanoparticles, such as C_{70} (size ∼ 1.2 nm) and gold particles (size 6–10 nm), can be easily transported from vascular root to above-ground tissue.[48,49] However, owing to their relatively larger particle size, the $BiF_3:Eu^{3+}$ nanoparticles could not move to other tissues of the rice and were accumulated in the division and differentiation regions of the rice root. As a consequence, the RFP signal was only detected in the division and differentiation regions of the rice root.
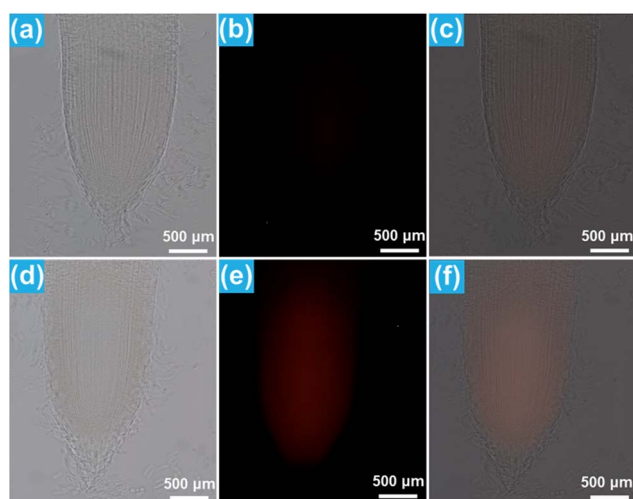

Fig. 5 Images of the rice root tip grown in the MS0 medium without adding nanoparticles with excitation at 396 nm: (a) bright channel, (b) RFP channel, and (c) merged channel. Images of the rice root tip grown in the MS0 medium treated with $BiF_3:Eu^{3+}$ nanoparticles with excitation at 396 nm: (d) bright channel, (e) RFP channel, and (f) merged channel.
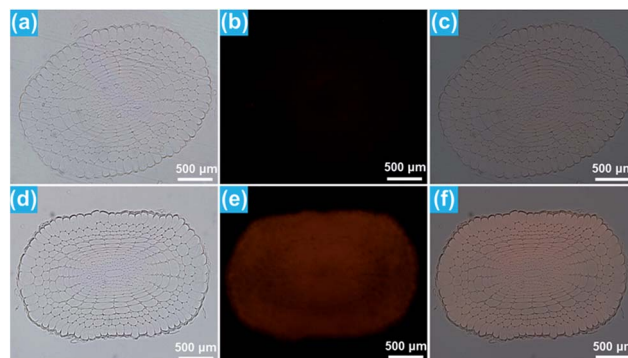

Fig. 6 Cross-sectional images of the rice root tip grown in the MS0 medium without adding nanoparticles with excitation at 396 nm: (a) bright channel, (b) RFP channel, and (c) merged channel. Cross-sectional images of the rice root tip grown in the MS0 medium treated with $BiF_3:Eu^{3+}$ nanoparticles with excitation at 396 nm: (d) bright channel, (e) RFP channel, and (f) merged channel.

4.   Conclusions

In summary, under excitation at 391 nm, the studied samples exhibited the characteristic emissions of Eu^{3+} ions. On raising the temperature, the FIR values of the emissions arising from the thermally coupled levels of $^5D_1$ and $^5D_0$ increased gradually. The maximum sensor sensitivity of the prepared samples was determined to be 3.4×10^{-5} K^{-1} at 443 K. Furthermore, after treatment with the $BiF_3:Eu^{3+}$ nanoparticles, the elongation of the primary root and the crown root number of the seedlings scarcely changed in comparison with those of the rice root grown in the MS0 medium without nanoparticles, revealing that the resultant nanoparticles exhibited relatively low phytotoxicity. In addition, the results of both the phenotype and toxicity-related gene levels also confirmed that the Eu^{3+}-activated BiF_3 nanoparticles showed low phytotoxicity to the rice root. Ultimately, under irradiation of 396 nm light, the RFP signals were only observed in the division and differentiation regions of the rice root, implying that the introduced nanoparticles could not be transferred from the vascular to the above-ground tissues and were only accumulated in the division and differentiation regions of the rice root. From these results, the Eu^{3+}-activated BiF_3 nanoparticles are expected to be a promising candidate for optical temperature sensors and fluorescence probes in plant cells.

Conflicts of interest

There are no conflicts to declare.

Acknowledgements

Notes and references

1 X. Huang, *Nat. Photonics*, 2014, **8**, 748–749.

2 P. Du and J. S. Yu, *Chem. Eng. J.*, 2017, **327**, 109–119.

3 J. Xu, P. Yang, M. Sun, H. Bi, B. Liu, D. Yang, S. Gai, F. He and J. Lin, *ACS Nano*, 2017, **11**, 4133–4144.

4 Y. Zheng, H. Zhang, W. Li, Y. Liu, X. Zhang, H. Liu and B. Lei, *RSC Adv.*, 2017, **7**, 33459–33465.

5 S. Hu, X. Wu, Z. Chen, P. Hu, H. Yan, Z. Tang, Z. Xi and Y. Liu, *Mater. Res. Bull.*, 2016, **73**, 6–13.

6 G. Kakavelakis, K. Petridis and E. Kymakis, *J. Mater. Chem. A*, 2017, **5**, 21604–21624.

7 X. Wang, Z. Zhao, Q. Wu, Y. Li and Y. Wang, *Inorg. Chem.*, 2016, **55**, 11072–11077.

8 H. Suo, X. Zhao, Z. Zhang and C. Guo, *ACS Appl. Mater. Interfaces*, 2017, **9**, 43438–43448.

9 J. Zhong, D. Chen, Y. Yuan, L. Chen, H. Yu and Z. Ji, *Chem. Eng. J.*, 2017, **309**, 795–801.

10 P. Du, L. Luo, H. Park and J. S. Yu, *Chem. Eng. J.*, 2016, **306**, 840–848.

11 J. Zhou, Z. Xia, M. Bettinlli and Q. Liu, *RSC Adv.*, 2016, **6**, 2046–2054.

12 X. Li, X. Chen, S. Yuan, S. Liu, C. Wang and D. Chen, *J. Mater. Chem. C*, 2017, **5**, 10201–10210.

13 X. Huang, H. Guo and B. Li, *J. Alloys Compd.*, 2017, **720**, 29–38.

14 Y. Tian, B. Tian, C. Cui, P. Huang, L. Wang and B. Chen, *Opt. Lett.*, 2014, **39**, 4164–4167.

15 W. Zhang, Y. Shen, M. Liu, P. Gao, H. Pu, L. Fan, R. Jiang, Z. Liu, F. Shi and H. Lu, *ACS Appl. Mater. Interfaces*, 2017, **9**, 39985–39993.

16 P. Du, X. Huang and J. S. Yu, *Chem. Eng. J.*, 2018, **337**, 91–100.

17 X. Zhao, H. Suo, Z. Zhang, L. Zhang and C. Guo, *Dyes Pigm.*, 2017, **146**, 119–126.

18 Y. Tian, Y. Tian, P. Huang, L. Wang, Q. Shi and C. Cui, *Chem. Eng. J.*, 2016, **297**, 26–34.

19 P. Du, A. M. Deng, L. Luo and J. S. Yu, *New J. Chem.*, 2017, **41**, 13855–13861.

20 J. Grube, *J. Lumin.*, 2016, **179**, 107–113.

21 S. Sarkar, A. Dash and V. Mahalingam, *Chem.–Asian J.*, 2014, **9**, 447–451.

22 L. Nie, Y. Shen, X. Zhang, X. Wang, B. Liu, Y. Wang, Y. Pan, X. Xie, L. Huang and W. Huang, *J. Mater. Chem. C*, 2017, **5**, 9188–9193.

23 A. Nicol, K. Wong, R. T. K. Kwok, Z. Song, N. Li and B. Z. Tang, *ACS Appl. Mater. Interfaces*, 2017, **9**, 28298–28304.

24 A. P. French, S. Mills, R. Swarup, M. J. Bennett and T. P. Pridmore, *Nat. Protoc.*, 2008, **3**, 619–628.

25 Q. Zhang, H. Sun, T. Kuang, R. Xing and X. Hao, *RSC Adv.*, 2015, **5**, 4707–4715.

26 S. Hu, X. Wu, Z. Chen, P. Hu, H. Yan, Z. Tang, Z. Xi and Y. Liu, *Mater. Res. Bull.*, 2016, **73**, 6–13.

27 J. Yi and G. An, *J. Plant Biol.*, 2013, **56**, 85–90.

28 S. Sabatini, D. Beis, H. Wolkenfelt, J. Murfett, T. Guilfoyle, J. Malamy, P. Benfey, O. Leyser, N. Bechtold, P. Weisbeek and B. Scheres, *Cell*, 1999, **99**, 463–472.

29 J. Yoon, L. H. Cho, S. L. Kim, H. Choi, H. J. Koh and G. An, *Plant J.*, 2014, **79**, 717–728.

30 J. Yang, S. Lee, R. Hang, S. R. Kim, Y. S. Lee, X. Cao, R. Amasino and G. An, *Plant J.*, 2013, **73**, 566–578.

31 X. Huang, B. Li, H. Guo and D. Chen, *Dyes Pigm.*, 2017, **143**, 86–94.

32 X. Liu, W. Xie, Y. Lü, J. Feng, X. Tang, J. Lin, Y. Dai, Y. Xie and L. Yan, *Inorg. Chem.*, 2017, **56**, 13829–13841.

33 X. Li, D. Xu, X. Liu and H. Guo, *RSC Adv.*, 2017, **7**, 53839–53845.

34 X. Wang, Q. Liu, Y. Bu, C. Liu, T. Liu and X. Yan, *RSC Adv.*, 2015, **5**, 86129–86236.

35 S. A. Wade, S. F. Collins and G. W. Baxter, *J. Appl. Phys.*, 2003, **94**, 4743–4756.

36 W. Chen, F. Hu, R. Wei, Q. Zeng, L. Chen and H. Guo, *J. Lumin.*, 2017, **192**, 303–309.

37 P. Du, L. Luo and J. S. Yu, *Part. Part. Syst. Charact.*, 2018, DOI: 10.1002/ppsc.201700416.

38 P. Du, L. Luo and J. S. Yu, *Microchim. Acta*, 2017, **184**, 2661–2669.

39 L. Marciniak, K. Prorok and A. Bednarkiewicz, *J. Mater. Chem. C*, 2017, **5**, 7890–7897.

40 L. Marciniak, A. Bednarkiewicz and W. Strek, *J. Lumin.*, 2017, **184**, 179–184.

41 P. Du, L. Luo and J. S. Yu, *J. Alloys Compd.*, 2018, **739**, 926–933.

42 Q. Min, W. Bian, Y. Qi, W. Lu, X. Yu, X. Xu, D. Zhou and J. Qiu, *J. Alloys Compd.*, 2017, **728**, 1037–1042.

43 W. Xu, X. Y. Gao, L. J. Zheng, Z. G. Zhang and W. W. Cao, *Sens. Actuators, B*, 2012, **173**, 250–253.

44 H. L. Wong, T. Sakamoto, T. Kawasaki, K. Umemura and K. Shimamoto, *Plant Physiol.*, 2004, **135**, 1447–1456.

45 J. Yuan, D. Chen, Y. Ren, X. Zhang and J. Zhao, *Plant Physiol.*, 2008, **146**, 1637–1650.

46 Y. Zhao, Y. Hu, M. Dai, L. Huang and D. Zhou, *Plant Cell*, 2009, **21**, 736–748.

47 C. D. Mai, N. T. Phung, H. T. To, M. Gonin, G. T. Hoang, K. L. Nguyen, V. N. Do, B. Courtois and P. Gantet, *Rice*, 2014, **7**, 30.

48 C. Lin, B. Fugetsu, Y. Su and F. Watari, *J. Hazard. Mater.*, 2009, **170**, 578–583.

49 Z. Zhu, H. Wang, B. Yan, H. Zheng, Y. Jiang, O. R. Miranda, V. M. Rotello, B. Xing and R. W. Vachet, *Environ. Sci. Technol.*, 2012, **46**, 12391–12398.